Int. J. Electrochem. Sci., 15 **(2020)** 3298 – 3314, doi: 10.20964/2020.04.40

International Journal of
ELECTROCHEMICAL
SCIENCE
www.electrochemsci.org

Galvanic Corrosion Behaviors of A508-III/304L Couples in Boric Acid Solution

Chenhao Sun[1], Yu Tan[1], Kuan He[2], Shenghan Zhang[1], Kexin Liang[1,], Quan Lu[1],*

[1] Hebei Key Lab of Power Plant Flue Gas Multi-Pollutants Control, Department of Environment Science and Engineering, North China Electric Power University, Baoding, 071003, PR China; Environmental Systems Optimization, College of Environmental Science and Engineering, North China Electric Power University, Beijing, 102206, PR China
[2].Huadian Water Engineering Co.,Ltd, Beijing, 100160, PR China
[*]E-mail: kexin91802@163.com

Received: 22 November 2019 / *Accepted:* 14 January 2020 / *Published:* 10 March 2020

Alloy 508-III steel and 304L stainless steel are often used in pressure vessels found in nuclear power plants, and when both are exposed to boric acid, galvanic corrosion will occur and affect operational safety. The corrosion behavior and galvanic corrosion behavior after pairing these two metals in different boric acid solutions were studied by open circuit potential, polarization curve, AC impedance, zero-resistance ammeter, weight loss and SEM methods. The results showed that the differences in electrochemical properties between the two metals made A508-III act as the anode and 304L act as the cathode to form a galvanic couple that promoted the occurrence of galvanic corrosion. Compared with a single corrosive environment, the corrosion rate of A508-III was significantly accelerated under galvanic corrosion and the surface oxide composition also changed. An increase in the concentration of boric acid solution exacerbated galvanic corrosion. An excessive anodic area could slow down the galvanic corrosion current and quickly stabilize the corrosion. Ultimately, a galvanic corrosion model of A508-III and 304L in boric acid solution was described.

Keywords: galvanic corrosion; A508-III steel; 304L stainless steel; electrochemistry; zero-resistance ammeter method

1. INTRODUCTION

Galvanic corrosion refers to corrosion behavior in which two or more metals having different potentials are in the same medium and conduct through a connection or other methods. The occurrence of galvanic corrosion is mainly due to metals having different open circuit potentials[1]. In the galvanic corrosion process, oxidation and reduction reactions involving free electrons and ions occur on the metal surface, including hydrogen depolarization and oxygen depolarization[2, 3]. Among them, the metal

material with a high potential value acts as a coupling cathode, and the surface generally undergoes a hydrogen evolution reaction and oxygen reduction reaction, which slows down the corrosion rate[4, 5]. The metal material with a low potential value serves as the coupling anode, the metal dissolves on the surface and the corrosion rate increases significantly[6].

The primary circuit pressure vessels of pressurized water reactor nuclear power plant often uses Alloy 508-III steel (A508-III) as the outer layer material and 304L stainless steel (304L) as the inner layer material[7]. Boric acid is used as a neutron absorber and lithium hydroxide is used as a pH regulator to control the reactivity in the water conditions[8]. Compared with 304L, A508-III has more active chemical properties. A508-III and 304L will form a galvanic couple when they are in the same solution medium, A508-III with a low corrosion potential will act as the anode and the corrosion rate accelerates. 304L with a high corrosion potential will act as the cathode, and the corrosion rate slows down. Boric acid, as a necessary neutron absorber in the primary circuit, is inherently corrosive to metals, especially when it leaks due to a rupture in the stainless steel shell and the failure of sealing elements in the primary circuit. The pH of the saturated boric acid solution at 95 ℃ is less than 3, which is extremely corrosive and causes dissolution and corrosion of carbon steel and low alloy steel[9-11]. In this case, because A508-III and 304L are simultaneously exposed to a high concentration of boric acid, they can potentially form galvanic couple, and accelerate the corrosion rate of the anodic metal, which will affect the safe operation of the nuclear power plant[12]. At present, there are few reports on galvanic corrosion in this situation.

Previous studies have shown that the factors affecting galvanic corrosion are complex, including material properties, galvanic couple geometry and environmental characteristics[1, 13, 14]. The corrosion potential difference between the two materials is the basis of galvanic corrosion. However, at the same time, the polarization of the metal material in the corrosive solution medium will also affect the degree of galvanic corrosion[15-17]. Among the geometric influencing factors, the area ratio of the anode and cathode has a great impact on galvanic corrosion. When the area ratio of the anode and cathode is large, the cathode current density is relatively small, and the dissolution rate of the anodic metal is fast[18-22]. On the other hand, the concentration, pH and temperature of the solution medium also greatly influence the galvanic corrosion rate[13, 23, 24].

In this study, the galvanic corrosion behaviors of an A508-III/304L coupled system is researched, and the influence of the solution concentration and area ratio on the galvanic corrosion of the A508-III/304L couple is investigated by using electrochemical methods, zero-resistance ammeter method, weight loss method and SEM analysis.

2. EXPERIMENTAL

2.1. Samples and solution preparation

Alloy 508-III steel and 304L stainless steel were selected as the experimental materials. The elemental compositions are shown in Table 1.

Table 1. Elemental composition of A508-III and 304L

	C	Si	Mn	P	S	Cr	Ni	Mo	Cu	Fe
A508-III	0.216	0.228	1.39	0.012	0.0031	0.122	0.068	0.54	0.117	Bal.
304L	0.03	0.52	1.03	0.017	0.006	18.01	9.60	-	-	Bal.

A508-III samples were processed into sizes of 10 mm×10 mm×4 mm, 20 mm×10 mm×4 mm, 50 mm×20 mm×4 mm and 40 mm×20 mm×4 mm; 304L samples were processed into sizes of 10 mm×10 mm×4 mm and 40 mm×20 mm×4 mm. Some 10 mm×10 mm×4 mm samples were used for electrochemical experiments, the 40 mm×20 mm×4 mm samples were used for weight loss experiments and the other samples were used for galvanic corrosion experiments. The backsides of the samples were soldered with wire and sealed with a sealing agent formulated from an epoxy resin and a curing agent (T31), leaving a surface as the working electrode. All samples were polished with wet silicon carbide metallographic sandpaper from 400 grit to 2000 grit. Then, they were cleaned with deionized water in an ultrasonic environment to remove surface impurities and washed with alcohol to remove surface oil. After drying with cold air, the cleaned samples were placed in a dry box filled with nitrogen.

In the primary circuit of nuclear power plants, boric acid is commonly used as a neutron absorber and lithium hydroxide is used as a pH regulator. To simulate the galvanic corrosion behavior of A508-III and 304L exposed to a boric acid leakage environment, different concentrations of analytical grade H_3BO_3 and $LiOH·H_2O$ were dissolved in deionized water as experimental solutions. The compositions of the solutions are shown in Table 2.

Table 2. Ionic compositions of the experimental solutions

Group	a	b	c
B (ppm)	1200	2400	6000
Li (ppm)	2	4	10

2.2. Electrochemical experiments

A traditional three-electrode system was used in the electrochemical experiments and carried out with a potentiostat. The reference electrode was a saturated calomel electrode (SCE), the auxiliary electrode was a platinum electrode and the working electrode was a sample. All potentials in the experiment were based on the SCE potential.

The experiments were carried out in a water bath at 25 °C, and the samples were immersed in boric acid solution for 30 min until the open circuit potential (OCP) was substantially stabilized. The potentiodynamic polarization scan started at 200 mV below the self-corrosion potential with a scan rate of 1 mV/s. The AC impedance measurements were taken at the self-corrosion potential, and the sine wave amplitude of the excitation signal was set to 5 mV with a frequency range of 10^6 Hz to 10^{-2} Hz. The measurement results were fitted and analyzed using ZSimpWin software.

2.3 Galvanic corrosion experiments

A zero-resistance ammeter method was applied in the galvanic corrosion experiments[25-27]. The A508-III and 304L samples were connected by a stainless steel wire and put into a boric acid solution; then, the galvanic voltage and current were monitored by a digital multimeter (Keithley 2000) at a temperature of 25 °C for 156 h. The working electrode area was set according to the experimental requirements, as shown in Table 3. The data at 1 h, 4 h, 8 h, and 24 h were recorded, and then they were recorded for every 12 h after the 24 h mark.

Table 3. Sample sizes of the materials selected for their different area ratios

area ratio	304L	A508-III
1:1	10×10×4 mm	10×10×4 mm
1:2	10×10×4 mm	20×10×4 mm
1:10	10×10×4 mm	50×20×4 mm

2.4. Weight loss experiments

Weight loss tests with the A508-III samples were carried out in a galvanic corrosion environment (area ratio 1:1) and a single corrosion environment. These tests were conducted in a 500-mL reactor kettle with different temperatures and different solutions; furthermore, three parallel samples were setup for each group. The samples were weighed and hung at the same height. High purity nitrogen gas was introduced into the kettle for 30 min before the experiment to reduce the effect of oxygen on the results. The samples were removed after 7 days and cleaned with water and a rust removing agent. Then they were blown dry with cold air and weighed. The corrosion rate of samples in the boric acid solution was calculated according to Eqn. (1)[21, 28]:

$$v = \frac{m_1 - m_2}{St} \quad (1)$$

where v represents the corrosion rate, g/(cm^2·d); m_1 is the mass before corrosion, g; m_2 is the mass after removal of the corrosion product, g; S is the sample surface area, cm^2 and t is the corrosion time, d.

2.5. Surface analysis

After the occurrence of galvanic corrosion for 156 h at 25 °C, the A508-III and 304L corrosion samples obtained under different solutions were subjected to SEM and EDS tests.

3. RESULTS

3.1. Open circuit potential (OCP)

The open circuit potential (OCP) of A508-III and 304L in boric acid solutions with different concentrations at 25 °C are shown in Fig. 1a and Fig. 1b, respectively. It can be seen that in different

concentrations of boric acid solution, the OCP of A508-III and 304L hardly changed with time. The OCP of A508-III was more stable, ranging from -0.67 V to -0.6 V, and for 304L it was -0.4 V to -0.05 V. The OCP values of the two materials increased with increasing solution concentration, while for 304L, it increased more obviously. The difference in OCP between the metals was greater than 0.3 V in all cases and became larger as the concentration of the solution increased. Serious galvanic corrosion occurred when the difference was greater than 250 mV, and the tendency of galvanic corrosion increased as the difference increased[29]. After coupling, A508-III with a low corrosion potential value acted as the anode and demonstrated accelerated corrosion, while 304L with a high potential value was protected as the cathode and demonstrated inhibited corrosion.

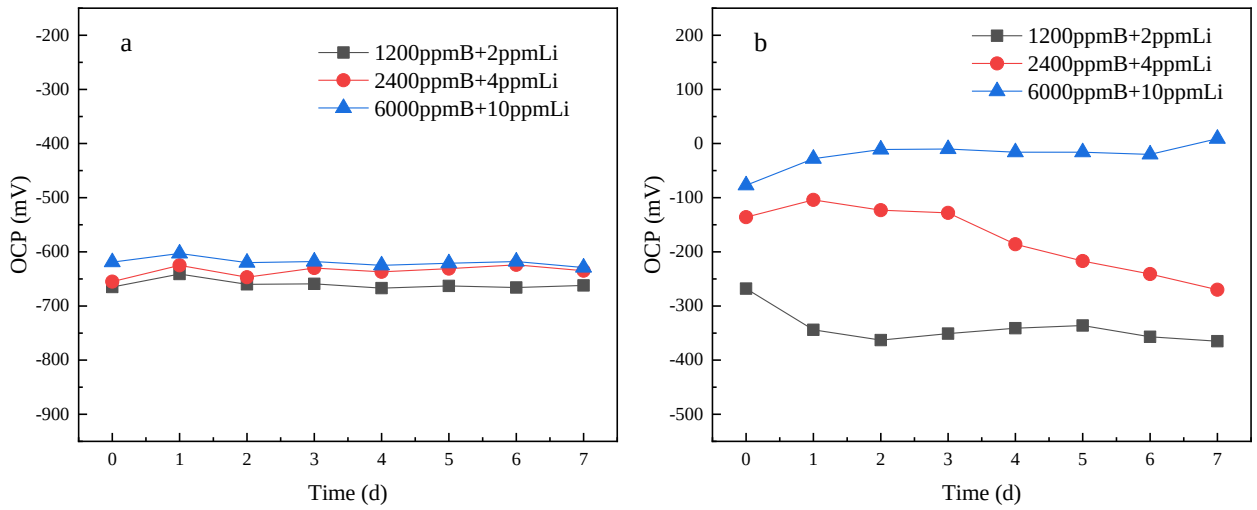

Figure 1. Open circuit potential (OCP) of a) A508-III and b) 304L with different concentration of boric acid and lithium ion solutions at 25°C

3.2. Polarization curve

The difference between the corrosion potentials provided the possibility of galvanic corrosion, but it was still necessary to consider the polarization of the metal material in the corrosive solution medium.

Fig. 2a and Fig. 2b show the respective potentiodynamic polarization curves of A508-III and 304L after immersion in different concentrations of solution for 30 min at 25 °C. The corrosion current density (I_{corr}) and passivation current density (I_p) of the corrosion samples were calculated by using the Tafel linear extrapolation method, as shown in Table 4. It could be observed that A508-III had no stable passivation zone in different concentrations of boric acid solution. In contrast, the 304L had a passivation phenomenon during the polarization process with a broad anodic polarization range.

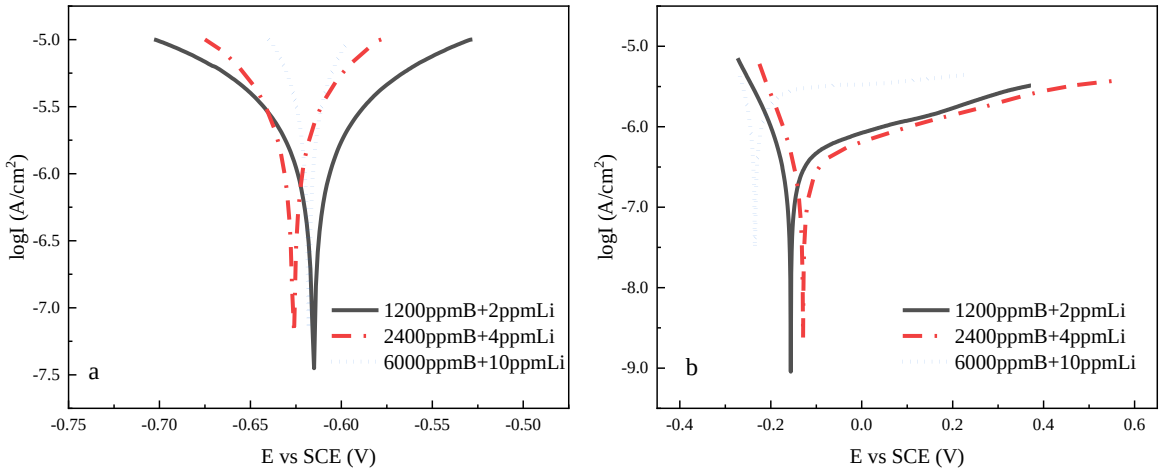

Figure 2. Polarization curves of a) A508-III and b) 304L with different concentrations of boric acid and lithium ion solutions at 25 °C

Due to the more active properties of A508-III, the corrosion current density was generally higher than that of 304L. As the concentration of the experimental solution increased, both materials exhibited greater corrosion current density. In addition, the passivation current density of 304L in boric acid solution was very small, indicating that its corrosion resistance in boric acid solution was relatively strong. With increasing solution concentration, the passivation current density of 304L increased slightly, which proved that the corrosion resistance of 304L in boric acid decreased with increasing solution concentration.

Table 4 Corrosion current density (I_{corr}) and passivation current density (I_p) of A508-III and 304L with different concentrations of boric acid and lithium ion solutions at 25 °C

	Solutions	Corrosion current density (I_{corr}) / A·cm^{-2}	Passivation current density (I_p) / A·cm^{-2}
A508-III	1200 ppm B+ 2 ppm Li	1.437E-06	None
	2400 ppm B+ 4 ppm Li	1.510E-06	None
	6000 ppm B+ 10 ppm Li	2.973E-06	None
304L	1200 ppm B+ 2 ppm Li	1.167E-07	7.129E-07
	2400 ppm B+ 4 ppm Li	1.928E-07	9.311E-07
	6000 ppm B+ 10 ppm Li	8.614E-07	3.126E-06

3.3. AC impedance

Fig. 3a and Fig. 3b show the respective Nyquist diagrams of A508-III and 304L after immersion in different concentrations of boric acid solution for 30 min. Fig. 4a and Fig. 4b show the Bode diagrams

of A508-III and 304L, respectively. It can be seen from the A508-III Nyquist diagram that two semicircular capacitive arcs were present in the boric acid solution, and these were found in the low frequency and high frequency regions; in contrast, 304L showed only one semicircular capacitive arc. In general, when the radius of the arc is large, the corrosion resistance of the material is high. As the concentration of the solution increased, the radius of the arcs for the A508-III and 304L samples gradually decreased, indicating a lower impedance; additionally, the corrosion tendency was intensified. It can be observed from the Bode diagram, the impedance modulus of A508-III decreased as the concentration of the solution increased at 0.01 Hz. In the 6000 ppm B+10 ppm Li solution, $|Z|_{0.01Hz}$ had a minimum value of approximately $2\times10^5\ \Omega$ and the phase angle was close to 0°; in contrast, 304L had the minimum impedance modulus in the 1200 ppm B+2 ppm Li solution, and the phase angle value was between 20~40°. The impedance modulus of 304L in the low frequency region was larger than that of A508-III.

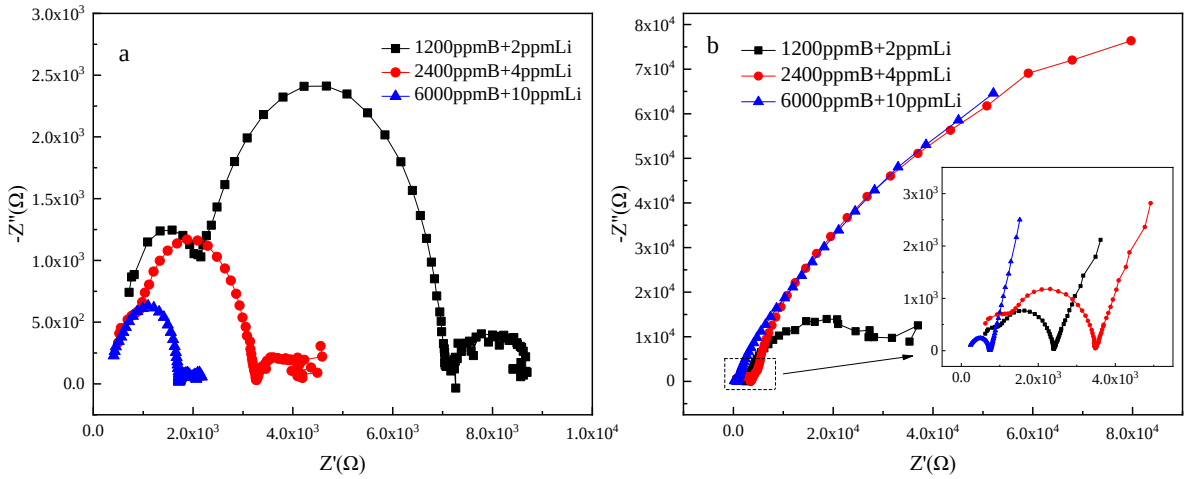

Figure 3. Nyquist diagrams of a) A508-III and b) 304L with different concentrations of boric acid and lithium ion solutions at 25 °C

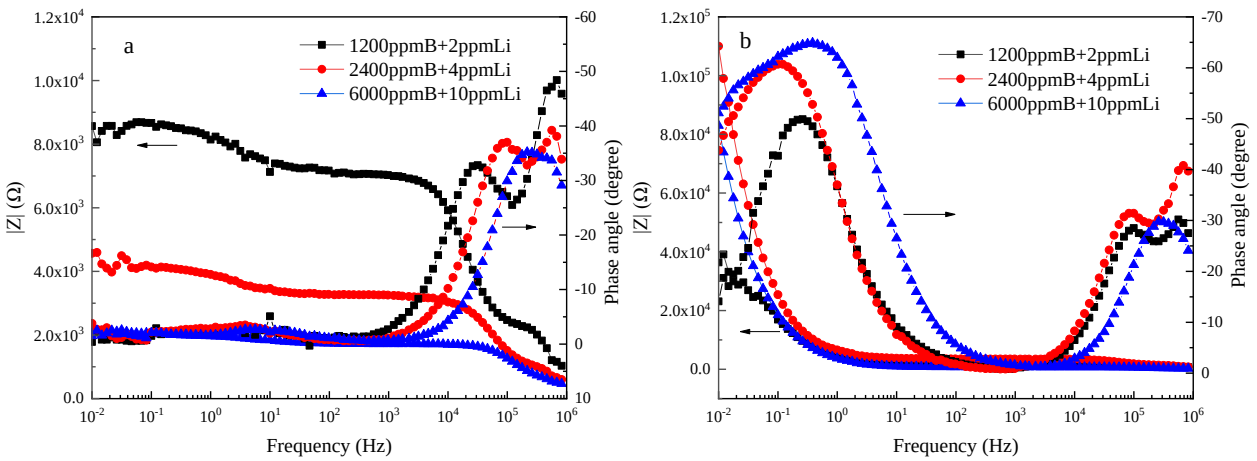

Figure 4. Bode diagrams of a) A508-III and b) 304L with different concentrations of boric acid and lithium ion solutions at 25 °C

The electrochemical impedance spectra of A508-III and 304L were fitted using the electrical equivalent circuit diagram in Fig. 5 by ZSimpWin software. The results are shown in Table 5. It can be seen from the fitting results that the transfer resistance (Rt) of A508-III was much smaller than that of 304L in a solution with the same concentration, indicating that 304L had better corrosion resistance than A508-III. The transfer resistance decreased as the concentration increased. It could also be concluded that 304L had a inferior dispersion effect.

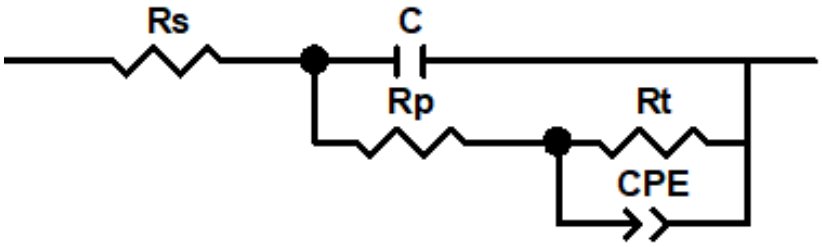

Figure 5. Electrical equivalent circuit diagram of A508-III and 304L with different concentrations of boric acid and lithium ion solutions

Table 5. Fitting parameters of AC impedance

Steel	Group	Rs(Ω)	C(F)	Rp (Ω)	CPE		Rt(Ω)
					Y	n	
A508-III	1200 ppm B+2 ppm Li	357.6	1.96E-10	2194	8.755E-9	0.8851	5246
	2400 ppm B+4 ppm Li	334.7	4.09E-10	913.1	7.561E-9	0.8791	2147
	6000 ppm B+10 ppm Li	401.8	1.014E-9	1273	0.001012	0.3426	555.5
304L	1200 ppm B+2 ppm Li	729.8	1.159E-9	1666	7.385E-5	0.7823	3.872E4
	2400 ppm B+4 ppm Li	826.0	7.37E-10	2616	5.863E-5	0.7792	2.528E5
	6000 ppm B+10 ppm Li	230.8	1.952E-9	501.9	7.558E-5	0.7713	2.130E5

3.4. Influence of area ratio on galvanic corrosion behavior

When the area ratios of the cathode (304L) and anode (A508-III) are 1:1, 1:2 and 1:10, the galvanic voltage and current of the galvanic couple in different concentrations of boric acid solution are shown in Fig. 6, Fig. 7 and Fig. 8, respectively.

As the reaction time progressed, the galvanic voltage and current gradually became stable, but the amount of time it took to reach stability under different area ratios was different. When the anodic area was large, the galvanic current stabilized more quickly. At the initial stage of the reaction, the surface of the metal quickly formed a passivation film in the galvanic corrosion environment. As the passivation film grew, the corrosion rate decreased, and the galvanic voltage and current also reached equilibrium. When the area ratio of the cathode and anode was 1:10, galvanic corrosion was stabilized within 24 h.

As the concentration of the solution increased, the steady-state galvanic corrosion voltage gradually increased. In a highly concentrated corrosive environment, the initial galvanic corrosion was

severe, resulting in a high corrosion current, but the stable corrosion current was independent of the solution concentration. The stable galvanic corrosion current in the solution of 1200 ppm B+2 ppm Li was the highest.

Taking the 1200 ppm B+2 ppm Li solution as an example, the increase of the anodic area increased the galvanic voltage in the steady-state, but the galvanic current did not increase accordingly. The stable current was similar when the area ratio was 1:1 or 1:2, and both were greater than that with the area ratio of 1:10. The current at the beginning of the reaction when the area ratio was 1:10 was smaller than in the other cases, which meant that an excessive anodic area suppressed the occurrence of galvanic corrosion. The initial current and steady current with the area ratio of 1:2 were the highest in all cases, and the current stayed at a high value during the first 18 h of the initial reaction, indicating that certain increases in the anodic area promoted galvanic corrosion.

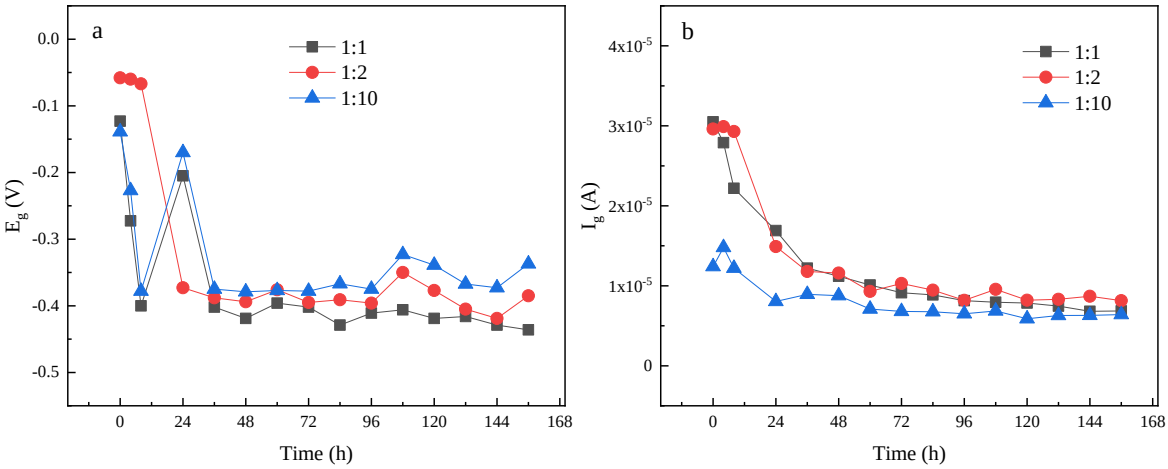

Figure 6. a) Galvanic voltages and b) galvanic currents of the galvanic couples with different area ratios in a 1200 ppm B+2 ppm Li solution for 156 h at 25 °C

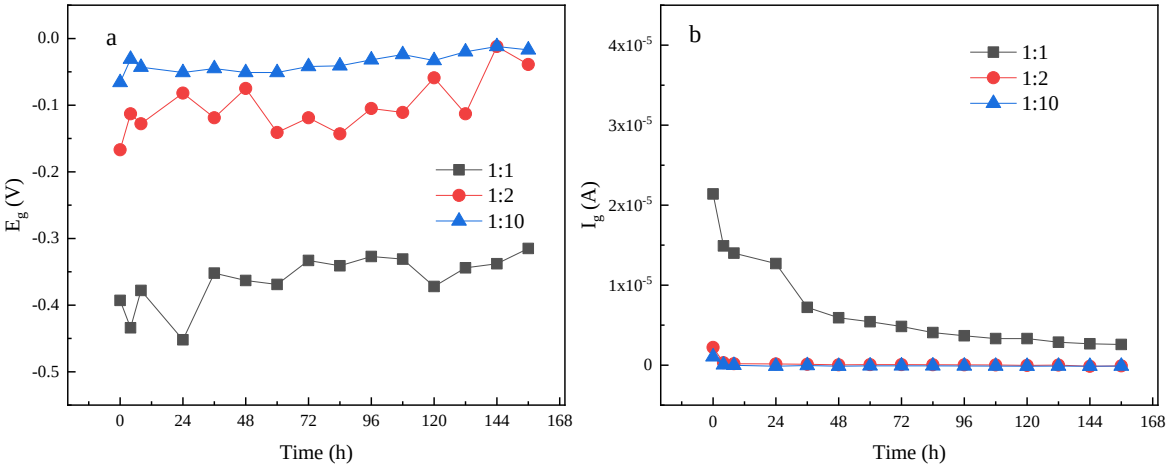

Figure 7. a) Galvanic voltages and b) galvanic currents of the galvanic couples with different area ratios in a 2400 ppm B+4 ppm Li solution for 156 h at 25 °C

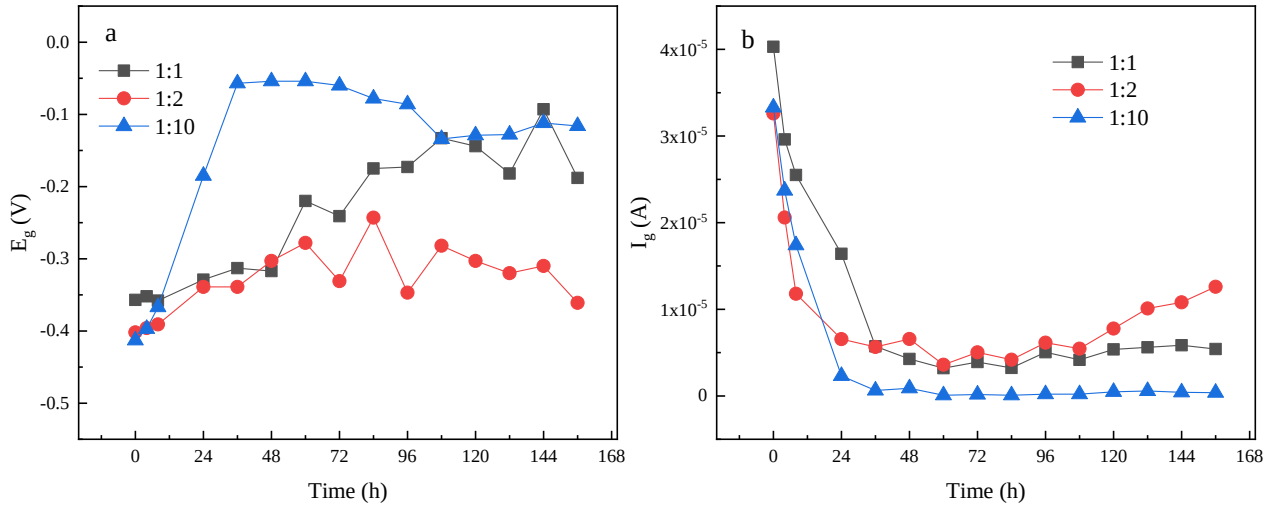

Figure 8. a) Galvanic voltages and b) galvanic currents of the galvanic couples with different area ratios in a 6000 ppm B+10 ppm Li solution for 156 h at 25 °C

Compared with other area ratios, the stable galvanic corrosion current was lowest with the 1:10 area ratio in any solution. At this area ratio, the cathode area was too small, and a large number of electrons from the anode could not accumulate on the cathode surface, thereby increasing the galvanic corrosion reaction resistance. The increase in the resistance of the solution also affected the galvanic current, and the galvanic current value was close to 0 in a highly concentrated boric acid solution.

3.5. Weight loss results

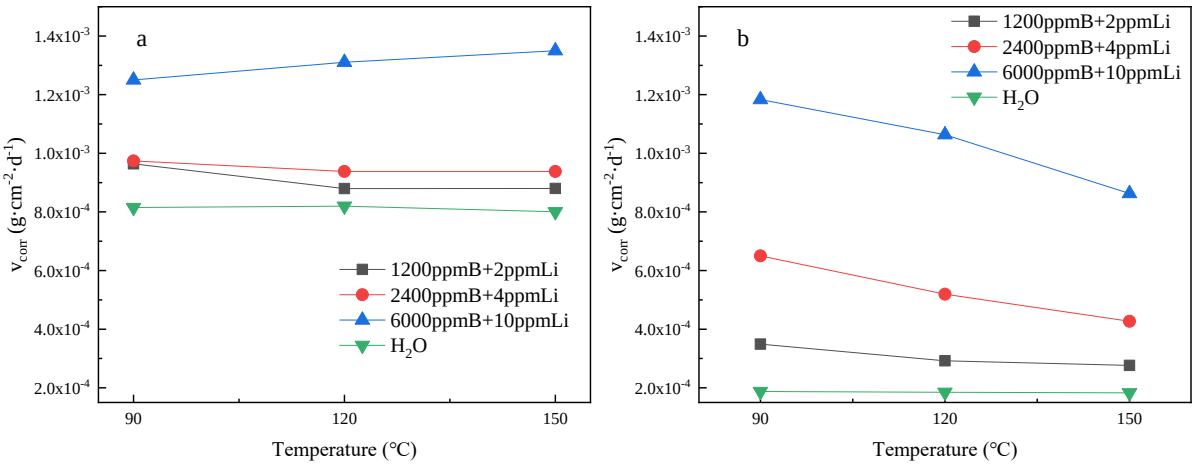

Figure 9. Corrosion rate of A508-III in solutions with different concentrations of boric acid and lithium ion under different temperatures in the a) galvanic corrosion environment and b) single corrosion environment

The corrosion rates of A508-III after 7 days of galvanic corrosion and single corrosion in solutions with different concentrations under different temperatures are shown in Fig. 9a and Fig. 9b, respectively. In both environments, as the concentration of the solution increased, the corrosion rate had the same increasing trend. Compared with the single corrosion results, the corrosion rate of A508-III was significantly increased after the formation of galvanic couples at the same temperature, which was due to A508-III acting as the anode, which accelerated corrosion during the galvanic corrosion process. A solution with low concentration made the galvanic corrosion acceleration effect more obvious. The influence of temperature on the galvanic corrosion rate was small. Only in the 6000 ppm B+4 ppm Li solution colud the increase in temperature properly accelerate the corrosion degree of A508-III. In fact, the influence of temperature on the galvanic corrosion rate was complicated. The corrosion process of A508-III in a boric acid solution mainly depended on the physical and chemical changes of the H-B-O system with temperature. In a boric acid solution, boric acid reacted with H_2O to form $[B(OH)_4]^-$, which was unstable at high temperatures; thus, the corrosion process depended on the temperature and the boron ion state. For low temperatures, the corrosion process of A508-III was the heat activation process, and the corrosion rate increased with increasing temperature, but when the temperature reached a high value, the corrosion rate might be determined by the content of H_3O^+ ions in the solution[30-33].

3.6. Morphology of the surface

Fig. 10 shows the SEM images of A508-III and 304L after galvanic corrosion for 156 h at 25 °C in different concentrations of solution. It can be seen from Fig.10a~ Fig.10d that after galvanic corrosion, the surface of A508-III was loose and porous, and the material distribution was uneven. As the concentration of corrosive solution increased, the amount of surface corrosion products increased.

The corrosion surface formed in the 6000 ppm B+10 ppm Li solution changed from a particle distribution to a bundle distribution. It can be seen from Fig. 10e~Fig. 10h, most of the corrosion products of A508-III were clusters of polyhedral structures, and an increase in the concentration of the solution made the diameter and volume of the oxide particles increase. In contrast, the surface of 304L was uniform and dense, and the oxidation products were mostly cubic structures of different sizes.

The product formed on the A508-III surface under this condition was subjected to EDS analysis, and the results are shown in Table 6. As the concentration of the solution increased, the content of oxygen in the surface corrosion product increased, and the content of iron decreased, indicating that the composition of the corrosion product changed. At this time, the corrosion degree of A508-III carbon steel was also high.

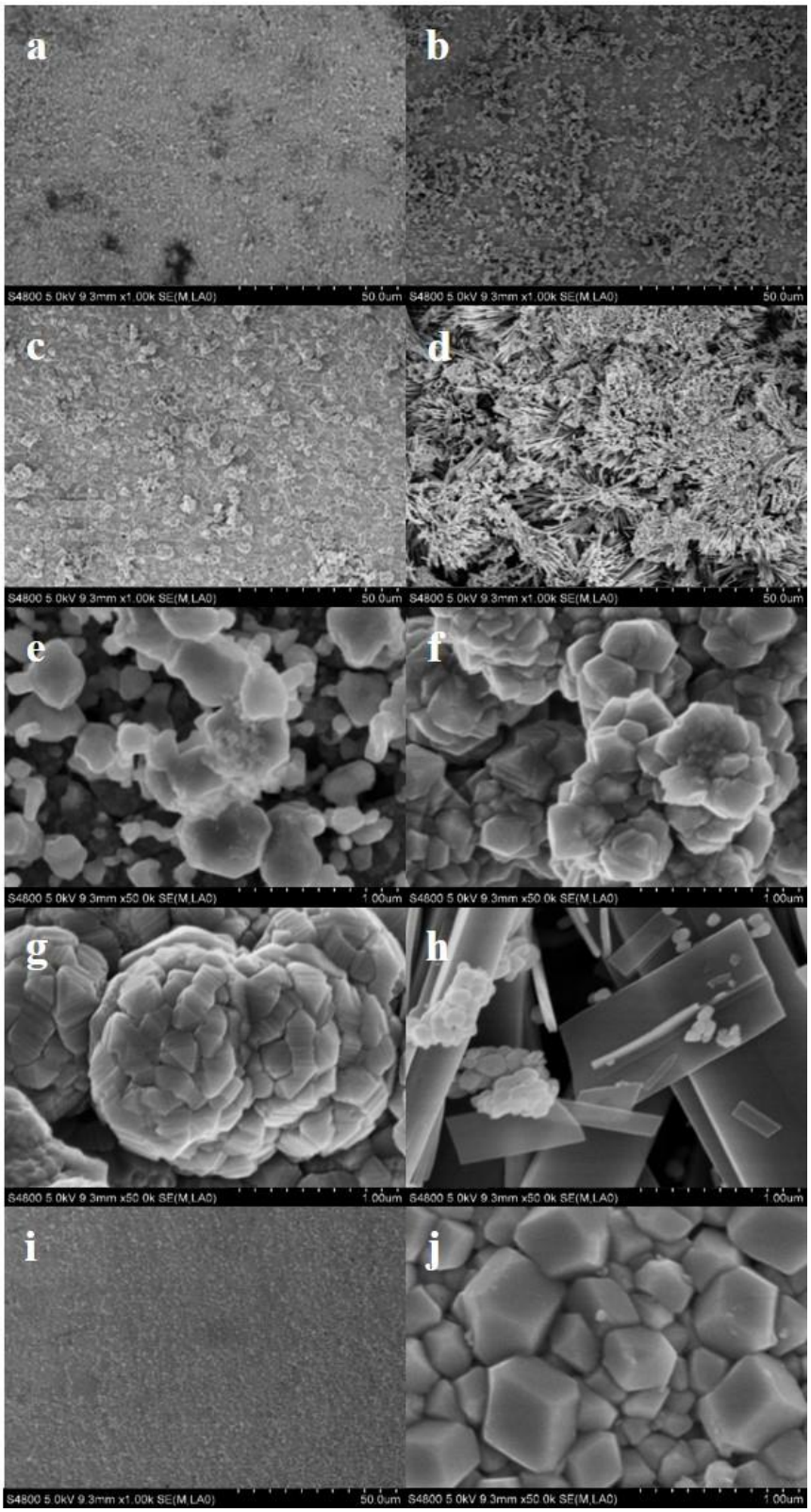

Figure 10. SEM images of A508-III and 304L after galvanic corrosion for 156 h at 25 °C with different concentrations of boric acid and lithium ion solutions: a) A508-III, H_2O, ×1.00k; b) A508-III, 1200 ppm B+2 ppm Li, ×1.00k; c) A508-III, 2400 ppm B+4 ppm Li, ×1.00k; d) A508-III, 6000 ppm B+10 ppm Li, ×1.00k; e) A508-III, H_2O, ×50.0k; f) A508-III, 1200 ppm B+2 ppm Li, ×50.0k; g) A508-III, 2400 ppm B+4ppm Li, ×50.0k; h) A508-III, 6000 ppmB+10 ppm Li, ×50.0k; i) 304L, 1200 ppm B+2 ppm Li, ×1.00k; and j) 304L, 1200 ppm B+2 ppm Li, ×50.0k

Table 6. EDS results of the products formed on A508-III after galvanic corrosion for 156 h at 25 °C

Group	Atomic percentage (at. %)		
	O	Mn	Fe
H2O	55.72	0.005	43.82
1200 ppm B+2 ppm Li	57.61	0	42.39
2400 ppm B+4ppm Li	58.46	0	41.54
6000 ppm B+10ppm Li	68.31	0	31.69

4. DISCUSSION

The open circuit potential (OCP) difference between A508-III and 304L was greater than 250 mV in all cases, and the OCP values of the two materials increased with increasing solution concentration, which provided the fundamental possibility for the occurrence of galvanic corrosion. The results of the polarization curves showed that A508-III had no stable passivation zone in all solutions, and an anodic polarization phenomenon was detected in 304L in the boric acid solution. As the solution concentration increased, the passivation current density increased slightly. Moreover, it could be concluded from the results of the AC impedance analysis that two semicircular capacitive arcs were involved in A508-III and only one semicircular capacitive arc was detected in 304L in the boric acid solution, and the transfer resistance of A508-III was much smaller than that of 304L in solutions with the same concentration. During the corrosion process, a passivation film was formed on the surface of 304L to reduce the corrosion rate and prevent corrosion. According to previous studies[34-37], this passivation film had a double-layer film structure, which was consistent with the electrical equivalent circuit diagram in the AC impedance analysis, and when it was used as the cathode of a galvanic pair, the formation of passivation film would be accelerated. While the surface of A508-III did not form a stable and dense passivation film during galvanic corrosion, but continuously accumulated different corrosion products and accelerated corrosion. The corrosion resistance of the two metals decreased as the concentration of the solution increased, which was due to the increase in the concentration of boric acid and lithium ions decreased the pH of solutions[38]. The results of the weight loss experiments showed that the corrosion rate of A508-III in the case of galvanic corrosion was much higher than that of single corrosion in the same solution. The combined analysis of these results confirmed the occurrence of galvanic corrosion between A508-III and 304L.

The galvanic corrosion processes with A508-III and 304L in boric acid solution are shown in Fig. 11. The A508-III anode in the couple was dissolved, and the reacted metal entered the boric acid solution as ions or hydrated ions and generated excess electrons on the metal surface; when the electrons reached the 304L cathode, they were absorbed by the reducing substance in the surface solution and underwent reduction reactions. The ions in the solution moved towards the oppositely charged region, that is, the cation moved towards the cathodic region, and the anion moved towards the anodic region, thereby forming a current loop[39-42]. The free B^{3+} in the solution combined with the OH^- precipitated from the cathode to form $[B(OH)_4]^-$, which increased the conductivity of the solution and accelerated the galvanic corrosion process. At this time, A508-III as the anode had a continuously increasing rate of

corrosion and formed corrosion products on the surface; in contrast, 304L as the cathode formed a dense passivation film on the surface, which slowed down the corrosion process. Increasing the corrosive solution concentration could accelerate the galvanic corrosion process, and the SEM and EDS results illustrated that the increase in concentration made the diameter and volume of the oxide particles on the surface of A508-III (as the anode) larger and exacerbated particle aggregation. The composition of the corrosion product also changed. These corrosion products and corrosion defects generated during galvanic corrosion could cause A508-III to perforate, fracture and cause safety accidents during service. While the surface of 304L still showed a flat and dense morphology after galvanic corrosion, and the presence of spinel substances could be observed on the passivation film. These substances had been proven in previous studies to effectively improve the corrosion resistance of materials, because they could be closely aligned and prevent the entry of oxygen[43-46].

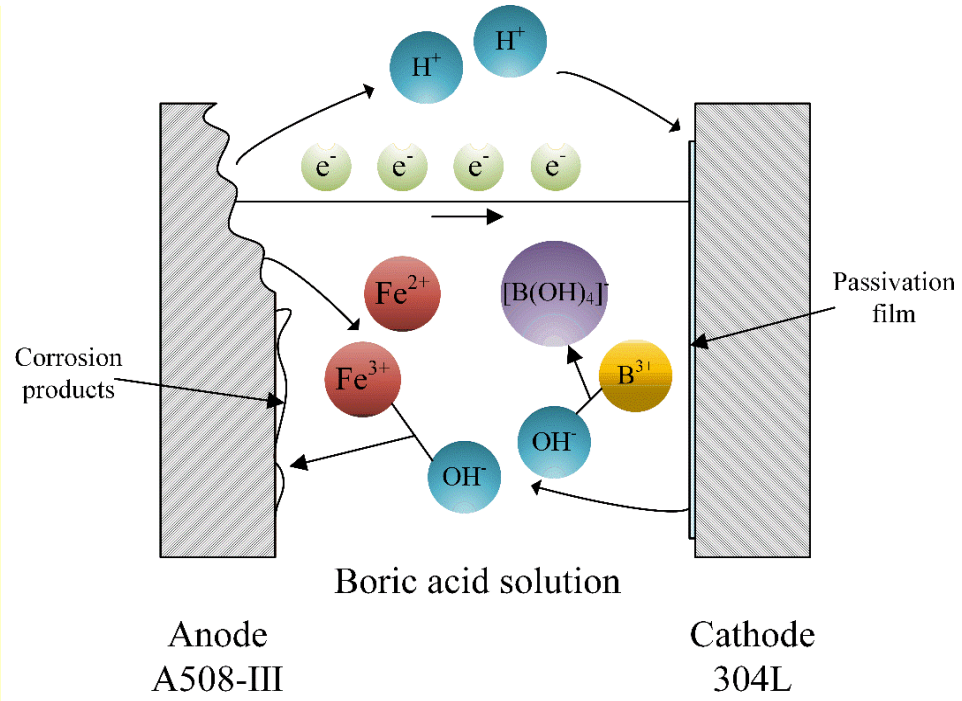

Figure 10. Schematic diagram of galvanic corrosion with A508-III and 304L coupled in boric acid solution

In the results of the area ratio influence on the degree of galvanic corrosion, it can be found that the increase in the anodic area could more quickly stabilize galvanic corrosion. Compared with previous research results[18, 19, 22, 24, 47], the area ratio of the cathode (304L) and anode (A508-III) was not a linear, positive correlation with the galvanic corrosion degree in boric acid solution, and an excessive anodic area inhibited galvanic corrosion. The galvanic voltage of the couple increased as the anodic area increased, but the galvanic current did not increase accordingly. This situation could be explained as follows. On the one hand, during hydrogen depolarization, the galvanic current density was controlled by the cathode current. A relatively small area of 304L increased the cathode current density. At this time, the hydrogen overvoltage of 304L increased, and the speed of hydrogen depolarization decreased, which slowed the dissolution of the A508-III anode. On the other hand, in the process of oxygen

depolarization, the galvanic corrosion current density was controlled by the diffusion of oxygen, and the relative decrease in the area of 304L reduced the oxygen content on the 304L surface, making it more difficult to carry out reduction reactions and reducing the galvanic current density[48-51]. In addition, the conductivity (resistance) in the solution under different area ratio conditions varied greatly, so the galvanic current did not increase in equal proportion. These results indicated that the principle governing the effect of the area ratio on the degree of galvanic corrosion was complicated. The area ratio, the ability to gain and to lose electrons and ions, and the conductivity of the corrosive solution synergistically affected galvanic corrosion, and the specific impacts of each need to be further explored.

In consideration of the fact that the nuclear power plant used A508-III as the outer layer material and 304L as the inner layer material, and the accident of boric acid leakage often occurred in nuclear power plants[52-54]. When boric acid leakage or other accidents occurred, these two metals would inevitably form a galvanic pair and cause galvanic corrosion. At this time, A508-III as the anode metal might cause pitting or even cracking in a short time, causing more serious safety accidents. This situation had not been studied before, but it was a huge hidden danger. Excessive increase in the area of A508-III could suppress galvanic corrosion but might not be applicable to actual operating conditions. Therefore, further research on mitigating galvanic corrosion in this situation was needed based on other galvanic geometric and environmental factors.

5. CONCLUSIONS

A508-III was more susceptible to corrosion in different concentrations of boric acid solution than 304L at room temperature. There was no passivation phenomenon in the corrosion process of A508-III, and two semicircular arcs were formed in the impedance spectrum. The corrosion of 304L in boric acid solution had an obvious passivation zone, and the impedance spectrum contained one semicircular arc. As the concentration of the solution increased, the two materials had high corrosion sensitivity. In the galvanic couples of A508-III and 304L, when compared to a single corrosion environment, A508-III as the anode demonstrated accelerated corrosion. In addition, when the anodic area (A508-III) was large, the galvanic system tended to become stable more quickly; moreover, the excessive anodic area slowed down the galvanic corrosion current. The increase in concentration of the boric acid solution exacerbated the galvanic corrosion degree of A508-III. The distribution of corrosion products on the surface of A508-III at high temperature was related to changes in elemental content, and the process of A508-III and 304L galvanic corrosion in boric acid solution was described according to the above analyses.

ACKNOWLEDGMENTS
This work is supported by the Fundamental Research Funds for the Central Universities (No. 2018QN092); the Natural Science Foundation of Beijing, China (Grant No.2192051).

References

1. X.W. Chen, J.H. Wu And J. Wang, *Corrosion Science & Protection Technology*, 22 (2010) 363.

2. R. Sánchez-Tovar, *Int. J. Electrochem. Sci.*, 6 (2011) 5550.
3. M. Schneider, K. Kremmer, C. Lammel, K. Sempf And M. Herrmann, *Corros. Sci.*, 80 (2014) 191.
4. G.L. Song, *Corros. Sci.*, 52 (2010) 455.
5. M.T. Montañés, *Int. J. Electrochem. Sci.*, 5 (2010) 1934.
6. L. Jiang, *Int. J. Electrochem. Sci.*, 11 (2016) 3577.
7. J. Spence And D.H. Nash, *Int. J Pres. Ves. Pip.*, 81 (2004) 89.
8. A.V. Morozov, A.V. Pityk, A.R. Sahipgareev And A.S. Shlepkin, *J. Phys.: Conf. Ser.*, 1105 (2018) 1.
9. E.H. Lee, K.M. Kim, H.P. Kim, U.C. Kim, J.H. Bae And C.W. Won, *Key Eng. Mater.*, 277-279 (2005) 649.
10. S. Zhang, *Int. J. Electrochem. Sci.*, 13 (2018) 3246.
11. Q. Xiao, Z. Lu, J. Chen, M. Yao, Z. Chen And A. Ejaz, *J. Nucl. Mater.*, 480 (2016) 88.
12. L. M. Quej-Aké, A. Contreras And J. Aburto, *Int. J. Electrochem. Sci.*, 13 (2018) 7416.
13. T.F. Cui, D.X. Liu, P.A. Shi, J.J. Liu, Y.H. Yi And H.L. Zhou, *Mater. Corros.*, 67 (2016) 72.
14. N.A. Al-Mobarak, A.M. Al-Mayouf And A.A. Al-Swayih, *Int. J. Electrochem. Sci.*, 3 (2008) 631.
15. A.Y. Musa, A.A. Al-Amiery And L.T. Tien, *Korean J. Chem. Eng.*, 29 (2012) 818.
16. Z. Shi, J. Jia And A. Atrens, *Adv. Eng. Mater.*, 14 (2016) 324.
17. C. Ren, *Int. J. Electrochem. Sci.*, 10 (2015) 4029.
18. C. Arya And P.R.W. Vassie, *Cem. Concr. Res.*, 25 (1995) 989.
19. X. Feng, *Int. J. Electrochem. Sci.*, 11 (2016) 5226.
20. Z.J. Wang, Y.M. Wang And C.L. Wang, *Mat. Sci. Eng. A-Struct.*, 322 (2018) 1.
21. W.A. Wesley, *Transactions of the Electrochemical Society*, 73 (1938) 539.
22. M.G. Pujar, *Int. J. Electrochem. Sci.*, 3 (2008) 44.
23. E. Blasco-Tamarit, A. Igual-Munoz And J.G. Antón, *Corros. Sci.*, 49 (2007) 4472.
24. D.L. Fleming, B.Y. Lum And A.K. Roy, Galvanic corrosion-effect of environmental and experimental variables. *Corrosion/99 Conference*, San Antonio, TX, 1998, 1.
25. K. Habib, *Optik*, 118 (2007) 296.
26. S.H. Lee, I.K. Lee, J.H. Seo, J.H. Jeon, H.H. Choe, K.W. Lee, J. Winkler, N. Reinfried And W. Knabl, *Sid Symposium Digest of Technical Papers*, 40 (2012) 1320.
27. J. Wolstenholme, *Br. Corros. J.*, 9 (1974) 116.
28. R. Sánchez-Tovar, M.T. Montañés And J. García-Antón, *Corros. Sci.*, 68 (2013) 91.
29. G. Hao, D.K. Zhang, C. Kai And Q.L. Wang, *Mater. Express.*, 4 (2014) 213.
30. Q. Xiao, Z. Lu And J. Chen, *Corrosion and Protection*, 480 (2016) 88.
31. C.A. Campbell, S. Fyfitch And D.T. Martin, Boric acid corrosion of carbon and low alloy steels, NACE International, (1994) Houston, TX, United States.
32. Q. Xiao, Z.P. Li, J.J. Chen, X.F. Xia And B.X. Zhou, *Corrosion & Protection*, 36 (2015) 294.
33. J. Ma, P. Li, W. Wang, S. Wang, X. Pan, F. Zhang, S. Li, S. Liu, H. Wang, G. Gao, B. Xu, Q. Yuan, H. Shen And H. Liu, *ACS Nano*, 12 (2018) 9022.
34. S. He, *Int. J. Electrochem. Sci.*, 13 (2018) 5832.
35. F. Mohammadi, T. Nickchi, M.M. Attar And A. Alfantazi, *Electrochim. Acta*, 56 (2011) 8727.
36. J.J. Kim And Y.M. Young, *Int. J. Electrochem. Sci.*, 8 (2013) 11847.
37. L. Jinlong And L. Hongyun, *Appl. Surf. Sci.*, 263 (2012) 29.
38. C.E. Dávalos, *Int. J. Electrochem. Sci.*, (2013) 9785.
39. X.Q. Du, Q. Yang, Y. Chen, Y. Yang And Z. Zhang, *T. Nonferr. Metal. Soc.*, 24 (2014) 570.
40. P. Yin, *Int. J. Electrochem. Sci.*, 14 (2019) 8479.
41. G. Song, B. Johannesson, S. Hapugoda And D. StJohn, *Corros. Sci.*, 46 (2004) 955.
42. R.M. Souto, Y. González-García, A.C. Bastos And A.M. Simoes, *Corros. Sci.*, 49 (2007) 4568.
43. S. Zhang, R. Shi And Y. Tan, *J. Alloys Compd.*, 711 (2017) 155.
44. E. Laouini, *Int. J. Electrochem. Sci.*, 4 (2009) 1074.
45. S. Zhang, R. Shi, Y. Chen And M. Wang, *J. Alloys Compd.*, 731 (2018) 1230.

46. Y. Zhang, L. Yuan, X. Zhang, J. Zhang, Z. Yue And L. Li, *Appl. Surf. Sci.*, 410 (2017) 99.
47. M.E. Ikpi, J. Dong And W. Ke, *Int. J. Electrochem. Sci.*, 10 (2015) 552.
48. Z.F. Yin, M.L. Yan, Z.Q. Bai, W.Z. Zhao And W.J. Zhou, *Electrochim. Acta*, 53 (2008) 6285.
49. L.B. Coelho, M. Taryba, M. Alves, M.F. Montemor And M.G. Olivier, *Electrochim. Acta*, 277 (2018) 9.
50. S. Wang, *Int. J. Electrochem. Sci.*, 11 (2016) 8797.
51. S. Wang, *Int. J. Electrochem. Sci.*, 10 (2015) 4393.
52. T. Li, Z. Zhi And C. Yan, *Advanced Materials Research*, 1081 (2014) 58.
53. Y.-I. Kim, D.-J. Yoon, S.-S. Lee, Y.H. Lee And K.-B. Kim, *NDT & E International*, 44 (2011) 311.
54. T.-W. Ni, Q. Ding, Z.-G. Yang, H.-L. Zheng And X. Lou, *Eng. Failure Anal.*, 92 (2018) 317